

# Role of Collective Mode for Optical Conductivity and Reflectivity in Quarter-Filled Spin-Density-Wave State

Yuh TOMIO\* and Yoshikazu SUZUMURA\*\*

*Department of Physics, Nagoya University, Nagoya 464-8602*

(Received )

Taking account of a collective mode relevant to charge fluctuation, the optical conductivity of spin-density-wave state has been examined for an extended Hubbard model with one-dimensional quarter-filled band. We find that, within the random phase approximation, the conductivity exhibits several peaks at the frequency corresponding to the excitation energy of the commensurate collective mode. When charge ordering appears with increasing inter-site repulsive interactions, the main peak with the lowest frequency is reduced and the effective mass of the mode is enhanced indicating the suppression of the effect of the collective mode by charge ordering. It is also shown that the reflectivity becomes large in a wide range of frequency due to the huge dielectric constant induced by the collective mode.

KEYWORDS: optical conductivity, collective mode, spin-density-wave, charge ordering, reflectivity, quarter-filled band, extended Hubbard model

## §1. Introduction

It has been well known that collective modes of the charge fluctuation play an important role to determine the property of density waves, e.g., the pinning of the density wave and the dynamics such as the optical conductivity in organic conductor.<sup>1,2,3,4,5)</sup>

The effect of the collective mode of density waves on the optical conductivity is found in the pronounced peak at zero frequency, which gives rise to a sliding motion of the density wave. The collective mode of the charge-density-wave (CDW) state leads to the zero-frequency peak of the conductivity, whose magnitude depends on the strength of the coupling to phonon. For the spin-density-wave (SDW) state, the conductivity is determined only by the collective mode where the full weight is given by the peak. Such a fact is well known only for the incommensurate density wave. The optical conductivity for incommensurate density waves has been extensively examined since the work by Lee, Rice and Anderson<sup>6)</sup> who calculated the conductivity by taking account of the collective mode for both CDW and SDW. The collective mode, which participates in the sliding motion of the CDW, has the effective mass enhanced by the electron-phonon interaction. For large effective mass, the dominant contribution to the conductivity comes from the single particle excitation. On the other hand, the conductivity of SDW state exhibits only the zero frequency peak with the unrenormalized electron mass, i.e., the contribution from the single particle excitation diminishes due to complete compensation with that of the collective mode and the collective mode determines the conductivity for all the frequencies. The conductivity of SDW has been calculated analytically by Takada.<sup>7)</sup> The

numerical calculation of the conductivity with the several electron-phonon interactions has been performed by Fenton and Ares.<sup>8)</sup> Virosztek and Maki<sup>9)</sup> examined the pinning effect and the optical conductivity by introducing the phase Hamiltonian.

The calculation of the conductivity for the commensurate case is complicated since all the higher harmonics of the density wave must be taken into account. For understanding the conductivity in the presence of the commensurability and interaction, it is useful to calculate a sum rule showing that the summation of the conductivity with respect to the frequency is equal to the average of the kinetic energy.<sup>10,11)</sup> The sum rule depends on the magnitude of the interaction except for the limit of the weak coupling of the interaction as seen from the incommensurate case. The exact numerical calculation for the extended Hubbard model at quarter-filling has shown the reduction of the averaged value.<sup>12)</sup> This indicates an enhancement of effective mass of density wave. The optical conductivity of the Hubbard model is further examined by introducing the dimerization, which has an effect of producing the charge gap.<sup>13)</sup> However the calculation of the optical conductivity based on the mean field theory is required for the SDW state since the exact calculation of one-dimensional system leads to the absence of the long range order.

The SDW state of organic conductors has been studied extensively in terms of the mean-field theory. In order to understand the experiment in organic conductors where SDW coexists with CDW,<sup>14,15)</sup> several authors<sup>16,17,18)</sup> have examined the ground state of the extended Hubbard model at quarter-filling. They have shown such a coexistence when the inter-site repulsive interaction becomes larger than the critical value. Based on the mean field ground state, the collective modes for charge fluctuation have been calculated where the charge gap of the collective mode vanishes at the onset of charge order-

\* E-mail: tomio@edu2.phys.nagoya-u.ac.jp

\*\* E-mail: e43428a@nucc.cc.nagoya-u.ac.jp

ing.<sup>19,20</sup>) This comes from the second order phase transition between two kinds of ground states. Thus it is of interest to examine a role of such a low lying excitation on the dynamical quantities. The optical conductivity at quarter-filling was calculated within the single particle excitation,<sup>21</sup>) and the effects of collective excitations on absorption spectra were studied by applying the random phase approximation to the systems with a finite size.<sup>22,23</sup>) The purpose of the present paper is to demonstrate such a role of collective mode for the optical conductivity and the reflectivity. Further we examine the effect of charge ordering, which may originate in intersite repulsive interaction.

In §2, formulation for the optical conductivity is given. Based on the mean-field ground state, the random phase approximation is applied to calculate the response function for the electric current. In §3, the optical conductivity is calculated numerically. The effective mass is estimated from the main peak of the conductivity. In §4, the effective mass of the collective mode is calculated in terms of the phase Hamiltonian, which is derived from the response function. The result is compared with that of §3. Based on the optical conductivity, we examine the dielectric constant and reflectivity in §5. The plasma frequency is calculated from the sum rule of the optical conductivity. The results is analyzed in terms of the collective mode with low lying excitation. In §6, the effect of dimerization on the conductivity and the effective mass is briefly discussed.

## §2. Formulation

We consider a one-dimensional extended Hubbard model given by  $H = H_0 + H_{\text{int}}$ , where  $H_0$  and  $H_{\text{int}}$  are respectively defined by

$$H_0 = - \sum_{j=1}^N \sum_{\sigma=\uparrow,\downarrow} (t - (-1)^j t_d) \left( C_{j\sigma}^\dagger C_{j+1,\sigma} + \text{h.c.} \right), \quad (2.1a)$$

$$H_{\text{int}} = \sum_{j=1}^N (U n_{j\uparrow} n_{j\downarrow} + V n_j n_{j+1} + V_2 n_j n_{j+2}). \quad (2.1b)$$

In the Hamiltonian,  $C_{j\sigma}^\dagger$  denotes a creation operator of an electron at the  $j$ -th site with spin  $\sigma = (\uparrow, \downarrow)$ ,  $n_j = n_{j\uparrow} + n_{j\downarrow}$  and  $n_{j\sigma} = C_{j\sigma}^\dagger C_{j\sigma}$ . A periodic boundary condition is taken, i.e.,  $C_{j+N,\sigma}^\dagger = C_{j\sigma}^\dagger$  with the total number of lattice site  $N$ . The quantity  $t$  denotes the transfer energy and  $t_d$  corresponds to the dimerization where  $t$  and the lattice constant are taken as unity. Quantities  $U$ ,  $V$  and  $V_2$  are the coupling constants for repulsive interactions of the on-site, the nearest-neighbor site and the next-nearest-neighbor site.

For a quarter-filled band, where the Fermi wave number is given by  $k_F = \pi/4$ , the mean-fields (MFs) representing SDW and CDW are written as ( $m = 0, 1, 2$  and  $3$ , and  $\text{sgn}(\sigma) = +(-)$  for  $\sigma = \uparrow(\downarrow)$ )

$$S_{mQ_0} = \frac{1}{N} \sum_{\sigma=\uparrow,\downarrow} \sum_{-\pi < k \leq \pi} \text{sgn}(\sigma) \left\langle C_{k\sigma}^\dagger C_{k+mQ_0,\sigma} \right\rangle_{\text{MF}}, \quad (2.2a)$$

$$D_{mQ_0} = \frac{1}{N} \sum_{\sigma=\uparrow,\downarrow} \sum_{-\pi < k \leq \pi} \left\langle C_{k\sigma}^\dagger C_{k+mQ_0,\sigma} \right\rangle_{\text{MF}}, \quad (2.2b)$$

where  $Q_0 (\equiv 2k_F = \pi/2)$  induces density waves with a periodicity of four lattices. The  $z$ -axis is taken as the quantized axis of the SDW ordered state. The expression  $\langle O \rangle_{\text{MF}}$  denotes an average of  $O$  taken by the MF Hamiltonian,<sup>18)</sup> which is expressed as

$$\begin{aligned} H_{\text{MF}} = & \sum_{0 < k \leq Q_0} \sum_{\sigma} \Psi_{\sigma}^{\dagger}(k) \overset{\leftrightarrow}{H}_{\text{MF}}^{\sigma}(k) \Psi_{\sigma}(k) \\ & + NU \left[ -\frac{1}{16} - \frac{1}{2} (|D_{Q_0}|^2 - |S_{Q_0}|^2) - \frac{1}{4} (D_{2Q_0}^2 - S_{2Q_0}^2) \right] \\ & + NV \left( -\frac{1}{4} + D_{2Q_0}^2 \right) + NV_2 \left( -\frac{1}{4} + 2|D_{Q_0}|^2 - D_{2Q_0}^2 \right), \end{aligned} \quad (2.3)$$

with  $\Psi_{\sigma}^{\dagger}(k)$  being the four component vector given by  $\Psi_{\sigma}^{\dagger}(k) = (C_{k\sigma}^\dagger, C_{k+Q_0,\sigma}^\dagger, C_{k+2Q_0,\sigma}^\dagger, C_{k+3Q_0,\sigma}^\dagger)$ . The MF Hamiltonian has the following matrix elements.

$$\left( \overset{\leftrightarrow}{H}_{\text{MF}}^{\sigma}(k) \right)_{mm} = -2t \cos(k + mQ_0) + U/4 + V + V_2, \quad (2.4a)$$

$$\begin{aligned} \left( \overset{\leftrightarrow}{H}_{\text{MF}}^{\sigma}(k) \right)_{m+1,m} &= \left( \frac{U}{2} - 2V_2 \right) D_{Q_0} - \text{sgn}(\sigma) \frac{U}{2} S_{Q_0} \\ &= \left( \overset{\leftrightarrow}{H}_{\text{MF}}^{\sigma}(k) \right)_{m,m+1}^*, \end{aligned} \quad (2.4b)$$

$$\begin{aligned} \left( \overset{\leftrightarrow}{H}_{\text{MF}}^{\sigma}(k) \right)_{m+2,m} &= \left( \frac{U}{2} - 2V + 2V_2 \right) D_{2Q_0} - \text{sgn}(\sigma) \frac{U}{2} S_{2Q_0} \\ &\quad + 2it_d \sin(k + mQ_0). \end{aligned} \quad (2.4c)$$

In the present case of quarter-filling, MFs can be rewritten as<sup>18)</sup>  $S_0 = 0$ ,  $D_0 = 1/2$ ,  $S_{Q_0} = S_{3Q_0}^* \equiv S_1 e^{i\theta}$ ,  $D_{Q_0} = D_{3Q_0}^* \equiv D_1 e^{i(\theta - \pi/2)}$ ,  $S_{2Q_0} = S_{2Q_0}^* \equiv S_2$  and  $D_{2Q_0} = D_{2Q_0}^* \equiv D_2$ . Quantities  $S_1 (> 0)$ ,  $D_1 (\geq 0)$ ,  $S_2$  and  $D_2$  denote amplitudes for  $2k_F$  SDW,  $2k_F$  CDW,  $4k_F$  SDW and  $4k_F$  CDW, respectively. The quantity  $\theta$  denotes a phase of SDW. The phase diagram of the ground state on the plane of  $V$  and  $V_2$  has been shown explicitly in the previous paper.<sup>17,18,20</sup>) There are three kinds of ground state on the plane of  $V$  and  $V_2$  where respective order parameters are given by  $S_1$  in the region (I),  $S_1$  and  $D_2$  in the region (II) and  $S_1$ ,  $S_2$  and  $D_1$  in the region (III). The region (II) (region (III)) is given for large  $V$  ( $V_2$ ).

The MF Hamiltonian, eq. (2.3), is diagonalized with the eigenvalues  $E_l(k)$  ( $l=1,2,3$  and  $4$ ) and eigenvector  $|lk\sigma\rangle$  where four energy bands are defined as  $E_1(k) < E_2(k) < E_3(k) < E_4(k)$ . These quantities are given by,

$$\overset{\leftrightarrow}{H}_{\text{MF}}^{\sigma}(k) |lk\sigma\rangle = E_l(k) |lk\sigma\rangle, \quad (2.5a)$$

$$|lk\sigma\rangle_m = F_{lm\sigma}(k), \quad (2.5b)$$

where  $F_{lm\sigma}(k)$  is the component of the eigenvector. We note that only  $E_1(k)$  is occupied due to quarter-filling. The effect of commensurability of quarter-filling is sufficiently large in the present choice of  $U = 4$ , where the gap between  $E_1(k)$  and  $E_2(k)$  is much larger than the band width of  $E_1(k)$ .

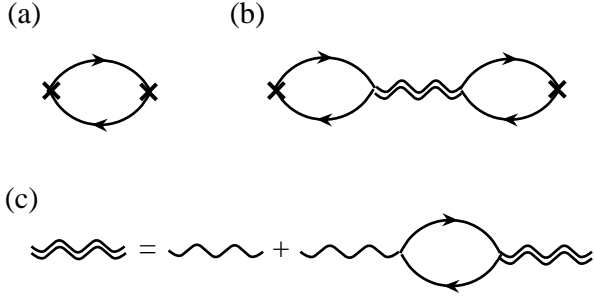


Fig. 1. Feynman diagram for the conductivity,<sup>6)</sup> where each lines consist of the basis of four components. The solid and wavy lines denote the electron Green function and the effective interaction, respectively and the cross denotes the current vertex. Respective diagrams denote (a) current-current response function for single particle excitation  $[\sigma_0(\omega)]$ , (b) current-current response function for collective mode  $[\sigma_c(\omega)]$  and (c) the effective interaction.

In order to examine the optical conductivity, we use the following lattice version.<sup>11)</sup> The current operator is expressed as

$$\begin{aligned}
 J &= ie \sum_{j\sigma} (t - (-1)^j t_d) (C_{j+1,\sigma}^\dagger C_{j\sigma} - C_{j\sigma}^\dagger C_{j+1,\sigma}) \\
 &= e \sum_{0 < k \leq Q_0, \sigma} \sum_{m=0}^3 \left( v_m(k) C_{k+mQ_0, \sigma}^\dagger C_{k+mQ_0, \sigma} \right. \\
 &\quad \left. - iu_m(k) C_{k+mQ_0, \sigma}^\dagger C_{k+(m+2)Q_0, \sigma} \right), \quad (2.6)
 \end{aligned}$$

where  $v_m(k) = 2t \sin(k + mQ_0)$  and  $u_m(k) = 2t_d \cos(k + mQ_0)$ . In terms of eqs. (2.6), the Kubo formula for the dynamical conductivity is given by

$$\sigma(\omega) + i\sigma'(\omega) = \frac{i}{N} \int_0^\infty dt e^{i\omega t} \langle [q(t), J(0)] \rangle, \quad (2.7)$$

where  $\sigma(\omega)$  and  $\sigma'(\omega)$  are real and  $q = e \sum_{j\sigma} j C_{j\sigma}^\dagger C_{j\sigma}$ . The optical conductivity is given by  $\sigma(\omega)$ . Within the random phase approximation, the real part of eq. (2.7) is calculated as<sup>6)</sup>

$$\sigma(\omega) = \sigma_0(\omega) + \sigma_c(\omega), \quad (2.8)$$

where  $\sigma_0(\omega)$  and  $\sigma_c(\omega)$  are respectively given by Fig. 1(a) and 1(b) as explained below. For the convenience of numerical calculation, we introduce a damping factor  $\eta$  by  $\omega \rightarrow \omega + i\eta$ . Thus a delta function corresponding to a pole is replaced by a peak with a finite width.

The first term of eq. (2.8) denotes the contribution from single particle excitation, which is written as [Fig. 1(a)]

$$\sigma_0(\omega) = \text{Re} \left\{ \frac{2}{i\omega} [\Pi_{jj}^0(\omega) - \Pi_{jj}^0(0)] \right\}, \quad (2.9)$$

where

$$\begin{aligned}
 \Pi_{jj}^0(\omega) &= \frac{1}{2N} \int_0^\beta d\tau \langle T_\tau J(\tau) J(0) \rangle_{\text{MF}} e^{i\omega_n \tau} \Big|_{i\omega_n \rightarrow \omega + i\eta} \\
 &= -\frac{e^2}{2N} \sum_{0 < k \leq Q_0, \sigma} \sum_{m_1, m_2} \sum_{l, l'} \frac{f(E_{l'}(k)) - f(E_l(k))}{\omega + i\eta + E_{l'}(k) - E_l(k)} \\
 &\quad \times [v_{m_1}(k) F_{lm_1\sigma}(k) - iu_{m_1}(k) F_{l, m_1+2, \sigma}(k)]
 \end{aligned}$$

$$\begin{aligned}
 &\times [v_{m_2}(k) F_{lm_2\sigma}^*(k) + iu_{m_2}(k) F_{l, m_2+2, \sigma}^*(k)] \\
 &\times F_{l', m_2\sigma}(k) F_{l', m_1\sigma}^*(k), \quad (2.10)
 \end{aligned}$$

and  $T_\tau$  is the ordering operator for the imaginary time  $\tau$ . The quantity  $\beta^{-1}$  denotes a temperature with the Boltzmann constant taken as unity and  $\omega_n = 2\pi n\beta^{-1}$  with integer  $n$ . The function  $f(x)$  denotes a Fermi distribution function given by  $[e^{(x-\mu)\beta} + 1]^{-1}$  where the chemical potential is given by  $\mu = (E_1(Q_0) + E_2(Q_0))/2$  in the limit of zero temperature. In deriving eq. (2.10), we used a single particle Green function (the solid line in Fig. 1), written as  $(\overleftrightarrow{G}^\sigma(k, i\omega_\nu))^{-1} = i\omega_\nu - \overleftrightarrow{H}_{\text{MF}}^\sigma(k) + \mu$  where  $\omega_\nu$  is the Matsubara frequency for Fermion.

The second term of eq. (2.8) denotes the contribution from the collective mode expressed as

$$\sigma_c(\omega) = \text{Re} \left\{ \frac{2}{i\omega} \Pi_{jj}^c(\omega) \right\}, \quad (2.11)$$

where

$$\begin{aligned}
 \Pi_{jj}^c(\omega) &= \frac{1}{2N} \int_0^\beta d\tau \langle T_\tau J(\tau) J(0) \rangle e^{i\omega_n \tau} \Big|_{i\omega_n \rightarrow \omega + i\eta} \\
 &= \hat{\Pi}_{ju}(\omega) \frac{\overleftrightarrow{U}(0)}{1 - \overleftrightarrow{U}(0) \overleftrightarrow{\Pi}(0, \omega)} \hat{\Pi}_{uj}(\omega). \quad (2.12)
 \end{aligned}$$

The matrix,  $\overleftrightarrow{U}(q)/(1 - \overleftrightarrow{U}(q) \overleftrightarrow{\Pi}(q, \omega))$ , denotes an effective interaction (Fig. 1(c)). The quantity,  $\overleftrightarrow{U}(q)$ , has only the diagonal element given by  $(\overleftrightarrow{U}(q))_{ii'} = \delta_{ii'} U_i(q)$ , ( $i = 1, 3, 0, 2$ ) where  $U_1(q) = U_3(q) = U$ ,  $U_0(q) = -(U + 4V \cos q + 4V_2 \cos 2q)$  and  $U_2(q) = -(U - 4V \cos q + 4V_2 \cos 2q)$ . In eq. (2.12), respective vector and matrix are written as

$$\hat{\Pi}_{ju}(\omega) = (\Pi_{jz}^{01}(\omega), \Pi_{jz}^{03}(\omega), \Pi_{jd}^{00}(\omega), \Pi_{jd}^{02}(\omega)), \quad (2.13)$$

$$\hat{\Pi}_{uj}(\omega) = (\Pi_{zj}^{10}(\omega), \Pi_{zj}^{30}(\omega), \Pi_{dj}^{00}(\omega), \Pi_{dj}^{20}(\omega))^t, \quad (2.14)$$

$$\overleftrightarrow{\Pi}(q, \omega) =$$

$$\begin{pmatrix}
 \Pi_{zz}^{11}(q, \omega) & \Pi_{zz}^{13}(q, \omega) & \Pi_{zd}^{10}(q, \omega) & \Pi_{zd}^{12}(q, \omega) \\
 \Pi_{zz}^{31}(q, \omega) & \Pi_{zz}^{33}(q, \omega) & \Pi_{zd}^{30}(q, \omega) & \Pi_{zd}^{32}(q, \omega) \\
 \Pi_{dz}^{01}(q, \omega) & \Pi_{dz}^{03}(q, \omega) & \Pi_{dd}^{00}(q, \omega) & \Pi_{dd}^{02}(q, \omega) \\
 \Pi_{dz}^{21}(q, \omega) & \Pi_{dz}^{23}(q, \omega) & \Pi_{dd}^{20}(q, \omega) & \Pi_{dd}^{22}(q, \omega)
 \end{pmatrix}, \quad (2.15)$$

The elements of eqs. (2.13)-(2.15) are calculated as

$$\begin{aligned}
 \Pi_{jz}^{0m}(\omega) &= \frac{1}{2N} \int_0^\beta d\tau \langle T_\tau J(\tau) S_{zm}^\dagger(0) \rangle_{\text{MF}} e^{i\omega_n \tau} \Big|_{i\omega_n \rightarrow \omega + i\eta} \\
 &= -\frac{e}{2N} \sum_{0 < k \leq Q_0, \sigma} \sum_{m_1, m_2} \sum_{l, l'} \frac{f(E_{l'}(k)) - f(E_l(k))}{\omega + i\eta + E_{l'}(k) - E_l(k)} \\
 &\quad \times [v_{m_1}(k) F_{lm_1\sigma}(k) - iu_{m_1}(k) F_{l, m_1+2, \sigma}(k)] \\
 &\quad \times F_{l, m_1+2, \sigma}^*(k) F_{l', m_2\sigma}(k) F_{l', m_1\sigma}^*(k) \text{sgn}(\sigma), \quad (2.16)
 \end{aligned}$$

$$\begin{aligned}
 \Pi_{zj}^{m0}(\omega) &= \frac{1}{2N} \int_0^\beta d\tau \langle T_\tau S_{zm}(\tau, 0) J \rangle_{\text{MF}} e^{i\omega_n \tau} \Big|_{i\omega_n \rightarrow \omega + i\eta} \\
 &= -\frac{e}{2N} \sum_{0 < k \leq Q_0, \sigma} \sum_{m_1, m_2} \sum_{l, l'} \frac{f(E_{l'}(k)) - f(E_l(k))}{\omega + i\eta + E_{l'}(k) - E_l(k)}
 \end{aligned}$$

$$\begin{aligned}
& \times [v_{m_2}(k)F_{l m_2 \sigma}^*(k) + i u_{m_2}(k)F_{l, m_2+2, \sigma}^*(k)] \\
& \times F_{l, m+m_1, \sigma}(k)F_{l' m_2 \sigma}(k)F_{l' m_1 \sigma}^*(k) \operatorname{sgn}(\sigma) , \\
\end{aligned} \tag{2.17}$$

and

$$\begin{aligned}
\Pi_{zd}^{mm'}(q, \omega) &= \Pi_{dz}^{mm'}(q, \omega) \\
&= \frac{1}{2N} \int_0^\beta d\tau \left\langle T_\tau S_{zm}(\tau, q) D_{m'}^\dagger(q) \right\rangle_{\text{MF}} e^{i\omega_n \tau} \Big|_{i\omega_n \rightarrow \omega + i\eta} \\
&= -\frac{1}{2N} \sum_{0 < k \leq Q_0, \sigma} \sum_{m_1, m_2} \sum_{l, l'} \frac{f(E_{l'}(k)) - f(E_l(k+q))}{\omega + i\eta + E_{l'}(k) - E_l(k+q)} \\
& \times F_{l, m+m_1, \sigma}(k+q) F_{l', m'+m_2, \sigma}^*(k+q) \\
& \times F_{l' m_2 \sigma}(k) F_{l m_1 \sigma}^*(k) \operatorname{sgn}(\sigma) , \\
\end{aligned} \tag{2.18}$$

where  $S_{zm}(q) = \sum_{k\sigma} C_{k\sigma}^\dagger C_{k+q+mQ_0, \sigma} \operatorname{sgn}(\sigma)$  and  $D_m(q) = \sum_{k\sigma} C_{k\sigma}^\dagger C_{k+q+mQ_0, \sigma}$ . Quantities  $\Pi_{jd}^{0m}(\omega)$ ,  $\Pi_{dz}^{m0}(\omega)$  and  $\Pi_{zz}^{mm'}(q, \omega) (= \Pi_{dd}^{mm'}(q, \omega))$  are given by eqs. (2.16), (2.17) and (2.18) without  $\operatorname{sgn}(\sigma)$ , respectively.

The spectrum of the collective mode is obtained from

$$\det \left( 1 - \overleftrightarrow{U}(q) \overleftrightarrow{\Pi}(q, \omega(q)) \right) = 0 , \tag{2.19}$$

where the basis vector is given by<sup>24)</sup>

$$\Phi(q) = (S_{z1}(q), S_{z3}(q), D_0(q), D_2(q))^t . \tag{2.20}$$

The solution of eq. (2.19) consists of several poles, i.e., isolated solution. We define  $\omega_c(q)$  as the pole with the lowest energy which corresponds to the mode leading to the sliding motion of density wave in the limit of weak interaction (or incommensurate case<sup>6)</sup>). In addition to  $\omega_c(0)$  expressing the charge fluctuation, some of other poles with higher energy may also give rise to the peak of the optical conductivity if they describe the charge fluctuation. In the next section, these mode are examined by rewriting the basis of eq. (2.20). In eq. (2.19), there are also three continua due to quarter-filled band, which contribute to the conductivity.

For calculating the effective mass, we note sum rules for  $\sigma(\omega)$  and  $\sigma_c(\omega)$  of eq. (2.8) expressed as

$$\int_0^\infty d\omega \sigma(\omega) = -\frac{\pi e^2}{2N} \langle H_0 \rangle_{\text{MF}} \equiv \frac{m}{m_c} \sqrt{2} e^2 , \tag{2.21}$$

$$\int_0^\infty d\omega \sigma_c(\omega) = 0 , \tag{2.22}$$

where  $m (= \pi/(4\sqrt{2}))$  is the band mass. In these equations, the former is known analytically<sup>10, 11)</sup> and the latter is verified numerically in the present paper. The mass,  $m_c$ , which is reduced to  $m$  for the incommensurate case, is renormalized by interactions. The effective mass of the collective mode can be obtained from the weight of the main peak of the conductivity.

### §3. Optical Conductivity

The frequency dependence of optical conductivity is examined to comprehend the role of the collective mode of the commensurate density wave at quarter-filling. Pa-

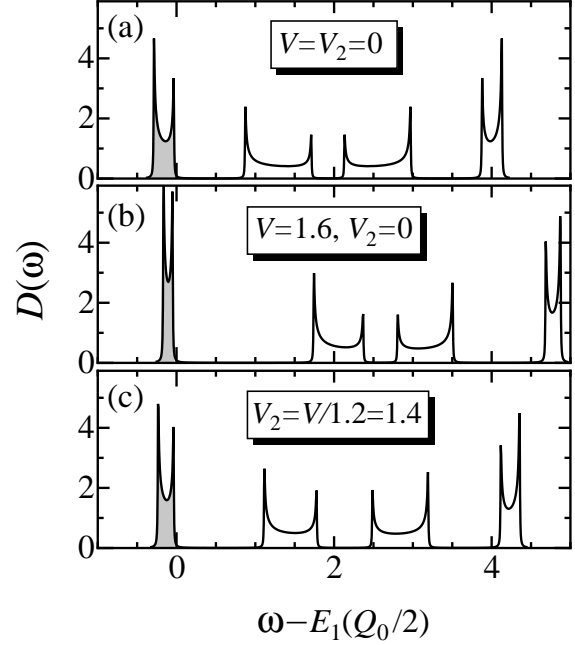


Fig. 2. The density of states for  $U = 4$ ,  $t_d = 0$  and with the fixed (a)  $V = V_2 = 0$  (region (I)), (b)  $V = 1.6$  and  $V_2 = 0$  (region (II)), and (c)  $V_2 = V/1.2 = 1.4$  (region (III)).

rameters  $U$ ,  $V$  and  $V_2$  are chosen as intermediate coupling e.g.  $U = 3, 4$  and  $5$ . We take  $t_d = 0$  in this section and discuss the effect of  $t_d \neq 0$  (i.e., dimerization) in the final section.

Since the fundamental contribution to the optical conductivity comes from the single particle excitation, we calculate the density of states defined by

$$D(\omega) = -\frac{2}{\pi N} \sum_{0 < k < Q_0} \operatorname{Im} \{ \operatorname{Tr} \overleftrightarrow{G}^\sigma(k, \omega + i0 - \mu) \} , \tag{3.1}$$

i.e.,  $D(\omega) = 2/(\pi N) \lim_{\delta \rightarrow +0} \sum_{k, \sigma} \sum_l \delta / ((\omega - E_l(k))^2 + \delta^2)$  where  $\int d\omega D(\omega) = 2$ . In Fig. 2, the density of states,  $D(\omega)$  is shown for  $U = 4$ , where three choices of parameters of  $V$  and  $V_2$  correspond to region (I), region (II) and region (III), respectively. The occupied states are shown by the shadow, the area of which is  $1/2$ . At quarter filling, density of states are divided into four parts, corresponding to  $E_1(k)$ ,  $E_2(k)$ ,  $E_3(k)$  and  $E_4(k)$ . There exists a symmetry with respect to  $\omega = (E_2(Q_0) + E_3(Q_0))/2$  only for  $V = V_2 = 0$ . The gap between the first band ( $E_1(k)$ ) and the second one ( $E_2(k)$ ) increases with increasing  $V$  and/or  $V_2$  while the second gap is nonmonotonical due to vanishing at  $V = U/4$  in the region (II) as seen from eqs. (2.4b) and (2.4c) with  $\theta = 0$ .

Now we calculate the optical conductivity. Figure 3 shows the conductivity for the Hubbard model with  $U = 3, 4$  and  $5$ , where dotted curve and solid curve correspond to  $\sigma_0(\omega)$  and  $\sigma(\omega)$ , respectively. The dotted curve shows the three continua, which correspond to the excitation from the filled (i.e., first) band to the second band, the third one and the fourth one. The solid curve exhibits three sharp peaks, which have the following relation to the spectrum of collective modes at  $q = 0$ . For  $U=4$ , the peaks are located at  $\omega \simeq 0.4, 3.0$  and  $4.8$

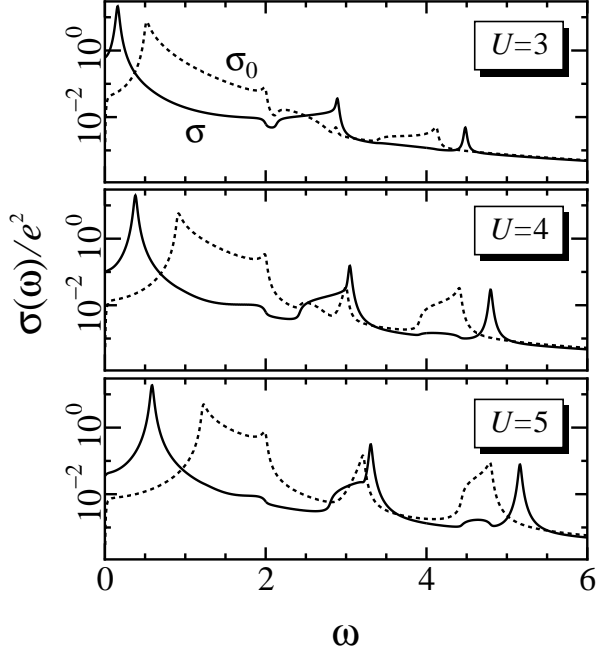


Fig. 3. Optical conductivity  $\sigma(\omega)$  is shown by the solid curve for  $U = 3, 4$  and  $5$  with  $V = V_2 = 0$ ,  $t_d = 0$  and  $\eta = 0.02$  where  $\sigma(\omega) = \sigma_0(\omega) + \sigma_c(\omega)$  and the dotted curve denotes  $\sigma_0$ , the contribution from single particle excitation.

while eq. (2.19) with  $q = 0$  gives five poles at  $\omega = 0.38, 2.24, 3.05, 3.88$  and  $4.80$  respectively with three continua  $0.91 < \omega < 2.00$ ,  $2.42 < \omega < 3.01$  and  $3.91 < \omega < 4.42$ . It is found that the peaks of  $\sigma(\omega)$  correspond to the first, third and fifth poles. The contribution from the second and fourth poles is absent within the numerical accuracy of the present calculation. For  $U = 3$ , the second and third peaks of  $\sigma(\omega)$  are reduced. This indicates a fact that  $\sigma(\omega)$  in the limit of small  $U$  is reduced to that of the incommensurate case where all the contribution of  $\sigma(\omega)$  is given by the first peak with  $\omega \rightarrow 0$  and the contribution from the single particle (i.e.  $\sigma_0(\omega)$ ) compensates completely with that of  $\sigma_c(\omega)$ . With increasing  $U$ , the weight for the lowest peak decreases and the second and the third peaks increase together with the continuum especially in the frequency region just below the second peak.

The effect of  $V$  on  $\sigma(\omega)$  is examined in Fig. 4 for  $U=4$  and  $V_2 = 0$  where  $\sigma(\omega)$  with  $V = 0.4$  and  $1.6$  are compared with that of  $V = 0$ . The conductivity of the upper panel is the same as that of  $U = 4$  in Fig. 3. The region (II) is obtained for  $V > V_c (= 0.34)$  while the region (I) is obtained for  $V < V_c$ . For  $V = 0.4$  (the middle panel), the peaks are located at  $\omega \simeq 0.2$  and  $4.0$  while eq. (2.19) with  $q = 0$  gives four poles at  $\omega = 0.18, 2.21, 3.98$  and  $4.65$  respectively with three continua in the regions  $0.92 < \omega < 2.11$ ,  $2.28 < \omega < 2.93$  and  $4.00 < \omega < 4.48$ . Thus, the peaks of  $\sigma(\omega)$  correspond to the first and third poles. The effect of  $\sigma_c$  is small for intermediate frequencies. This may come from the fact that the gap between the second band and the third band (i.e.,  $E_2(0)$  and  $E_3(0)$ ) vanishes at  $V = U/4$  in the region (II) as seen from eq. (2.4c) and  $\theta = 0$ . For

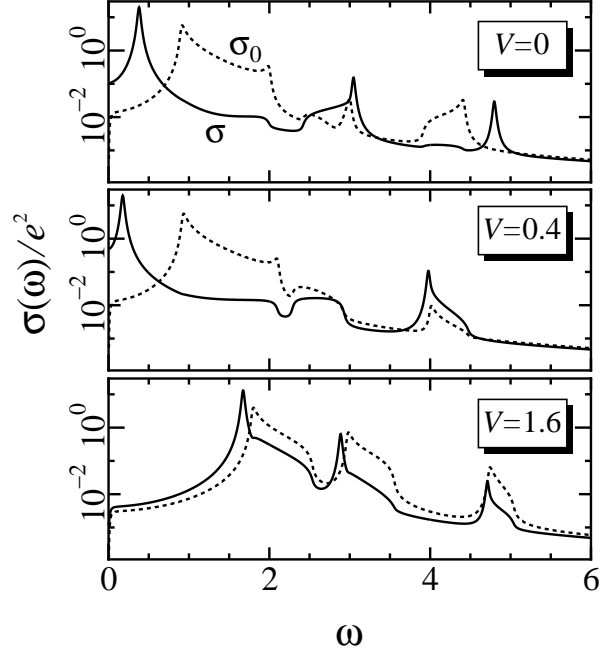


Fig. 4. Optical conductivity  $\sigma(\omega)$  is shown by the solid curve for  $V = 0, 0.4$  and  $1.6$  with  $U = 4$ ,  $V_2 = 0$ ,  $t_d = 0$  and  $\eta = 0.02$  where the notations are the same as Fig. 3.

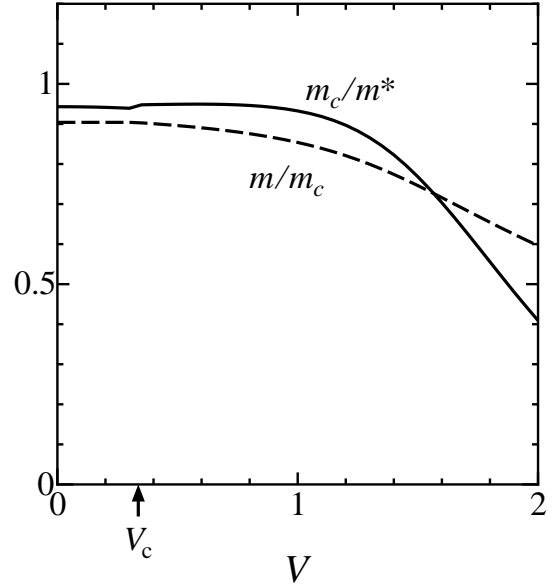


Fig. 5.  $V$  dependence of  $m/m_c$  (dashed curve) and  $m_c/m^*$  (solid curve) for  $U = 4$ ,  $V_2 = 0$  and  $t_d = 0$ . The ground state in the region (I) [region (II)] is obtained for  $V < V_c (\simeq 0.34)$  ( $V > V_c$ ).

$V = 1.6$  (the lower panel), the peaks are located at  $\omega \simeq 1.7, 2.9$  and  $4.7$  while eq. (2.19) with  $q = 0$  gives five poles at  $\omega = 1.67, 1.70, 2.89, 2.96$  and  $4.71$  respectively with three continua  $1.79 < \omega < 2.54$ ,  $2.97 < \omega < 3.56$  and  $4.74 < \omega < 5.04$ . Thus, the peaks of  $\sigma(\omega)$  correspond to first, third and fifth poles. It is found that, within the numerical accuracy, the second and fourth poles of the collective mode do not give the peak of the conductivity. With increasing  $V$ , the weight of the first peak is re-

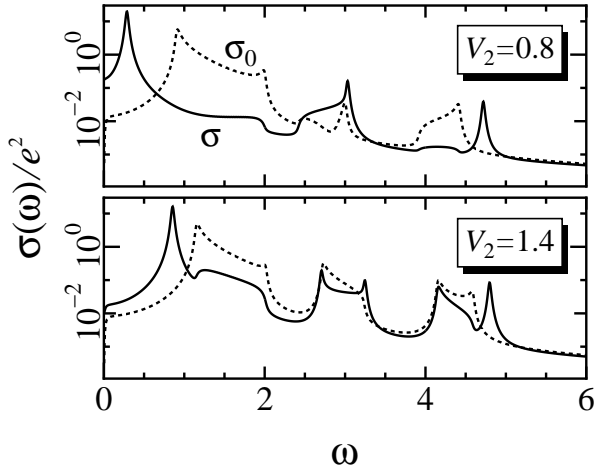


Fig. 6. Optical conductivity  $\sigma(\omega)$  is shown by the solid curve for  $V_2 = 0.8$  and  $1.4$  with  $U = 4$ ,  $V = 1.2V_2$ ,  $t_d = 0$  and  $\eta = 0.02$  where the notations are the same as Fig. 3.

duced. For large  $V$ , the compensation of the continuum by  $\sigma_c(\omega)$  is reduced and the continuum of  $\sigma(\omega)$  becomes noticeable.

Here we examine the total weight of the conductivity. In Fig. 5, the quantity  $m/m_c$  defined by eq. (2.21) as the function of  $V$  is shown by the dashed curve where  $m_c$  increases with increasing  $V$  due to narrowing of the filled band. Note that  $m/m_c = 1$  in the limit of small  $U$  and  $V$ . Here we examine the effect of  $V$  on the weight of the main (i.e., first) peak of  $\sigma(\omega)$ . Since the finite imaginary part  $\eta$  is introduced by treating  $\omega \rightarrow \omega + i\eta$ , we calculate the weight using a method given by

$$\int_0^{\omega_0} d\omega \sigma_c(\omega) \equiv \frac{m}{m^*} \sqrt{2} e^2, \quad (3.2)$$

where  $\omega_0$  denotes the lowest value of  $\omega$  satisfying  $\sigma_c(\omega) = 0$ , i.e., the solid curve and the dotted curve in Fig. 4 cross each other at  $\omega = \omega_0$ . The quantity  $m^*$  may be regarded as the effective mass for the collective mode with the first (lowest) pole. In Fig. 5, the quantity  $m_c/m^*$ , which denotes a fraction of the collective mode is shown by the solid curve. With increasing  $V$ , the quantity  $m_c/m^*$  decreases indicating the decrease of the contribution from collective modes. There is a jump of  $m_c/m^*$  at  $V = V_c$ . In the limit of the weak coupling, one obtains  $m_c/m^* = 1$  showing that the conductivity is determined only by a collective mode with  $\omega \rightarrow 0$ .

The effect of  $V_2$  on the conductivity is examined in Fig. 6 with  $U = 4$  and  $V/V_2 = 1.2$ . Note that the parameter with  $V_2 = 0.8$  ( $V_2 = 1.4$ ) corresponds to the region (I) [region (III)] as seen from a fact that the boundary between region (I) and region (II) for  $U = 4$  is given by<sup>18)</sup>  $V \simeq V_2 + 0.34$  for  $V_2 < V_{2c}(= 1.32)$ . Since the ground state of  $V_2 = 0.8(= V/1.2)$  is the same as that of  $V = V_2 = 0$ , the dotted curve of  $V_2 = 0.8$  is the same as that of  $V = 0$  in Fig. 4 (and also  $U = 4$  in Fig. 3). However the solid curve deviates from that of  $V = 0$  due to  $\sigma_c(\omega)$ , which depends on not only  $U$  but also  $V$  and  $V_2$ . The peaks correspond to the first, third and fifth poles of the collective mode where their five poles located at

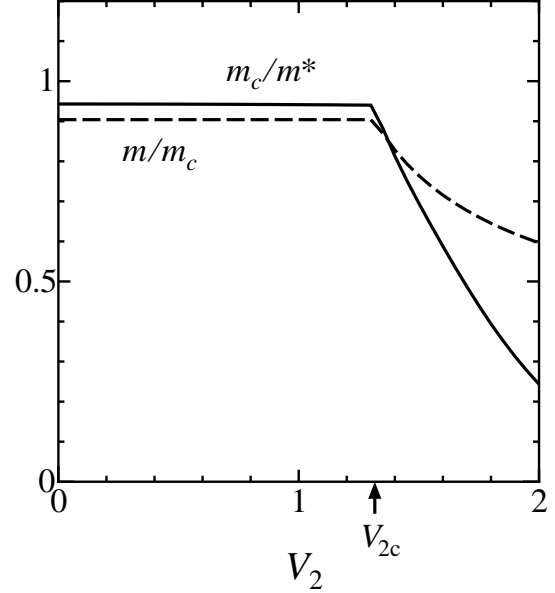


Fig. 7.  $V_2$  dependence of  $m/m_c$  and  $m_c/m^*$  for  $U = 4$ ,  $V = 1.2V_2$  and  $t_d = 0$ . The ground state in the region (I) [region (III)] is obtained for  $V_2 < V_{2c}(\simeq 1.32)$  ( $V > V_{2c}$ ).

$\omega = 0.29, 2.24, 3.03, 3.88$  and  $4.72$  are slightly different from those of Fig. 3 with  $U = 4$ . Such a small change of  $\sigma(\omega)$  is due to the effect of  $V_2$  on the charge fluctuation. For  $V_2 = 1.4$ , there appears five peaks located at  $\omega \simeq 0.9, 2.7, 3.2, 4.1$  and  $4.8$  while Eq. (2.19) with  $q = 0$  gives six poles at  $\omega = 0.85, 2.59, 2.71, 3.25, 4.12$  and  $4.80$  respectively with three continua  $1.15 < \omega < 2.01$ ,  $2.72 < \omega < 3.23$  and  $4.15 < \omega < 4.59$ . Thus, the peaks of  $\sigma(\omega)$  correspond to the first, third, fourth, fifth and sixth poles. We make following remarks as the effects of large  $V_2$ . The collective mode except for the second pole gives rise to the peak in the conductivity. The continuum of  $\sigma(\omega)$  which exists in the intermediate range of frequency is mainly determined by  $\sigma_0(\omega)$ , i.e., that of the single particle excitation. The contribution from the single particle excitation becomes dominant with increasing  $V_2$ .

Using the result of Fig. 6, we examine the  $V_2$  dependence of  $m_c/m^*$  and  $m/m_c$ , which are defined by eqs. (2.21) and (3.2). In Fig. 7,  $m_c/m^*$  and  $m/m_c$  as the function of  $V_2$  are shown by the solid curve and dashed curve respectively for  $U = 4$  and  $V/V_2 = 1.2$ . It is reasonable that  $m/m_c$  is constant for  $V < V_{2c}$ , i.e., region (I) since the quantity given by eq. (2.21) is determined only by the ground state. The quantity  $m/m_c$  (dashed curve) exhibits a cusp at  $V = V_{2c}$  but that of Fig. 5 is continuous at  $V = V_c$ . This fact is comprehended as follows. The ground state of region (III) is obtained by a competition between spin density ( $S_1$ ) and charge density ( $D_1$ ) while that of the region (II) (i.e., the coexistence with  $D_2$ ) is obtained mainly by the change of the phase of SDW. It is noticed that  $m_c/m^*$  is independent of  $V_2$  for  $V_2 < V_{2c}$  although the pole of the collective mode depends on  $V_2$ . The rapid increase of  $m^*$  for  $V_2 > V_{2c}$  shows a fact that the charge ordering ( $D_1 \neq 0$ ) induced by  $V_2$  enhances strongly the effective mass of the collec-

tive mode. For the case of varying  $V$  (the solid curve of Fig. 5), such an enhancement takes place for  $V$ , which is much larger than  $V_c$ . Thus it is found that charge ordering of  $D_2$  is less effective compared with that of  $D_1$ .

Here we note the relation between the peak of the conductivity and the pole of the collective mode. As mentioned in the previous section, the collective mode gives rise to the peak of the conductivity if it is optically active, i.e., the mode can describe the charge fluctuation. It is well known that, in the mode of the incommensurate case, the components of  $2k_F$  SDW and that of  $-2k_F$  SDW are the same in the magnitude but opposite in the sign.<sup>6)</sup> Extending the state to the present case of quarter-filling, we examined eq. (2.19) in the limit of small  $q$  by choosing a restricted two-component base as

$$\Phi(q) \rightarrow (e^{-i\theta} S_{z1}(q) - e^{i\theta} S_{z3}(q), D_2(q))^t. \quad (3.3)$$

We have verified that all the pole obtained from eq. (3.3) correspond to the location of the peak of the conductivity in Figs. 4 and 6. For the commensurate case, there are many poles describing the charge fluctuation while the pole with lowest energy gives the dominant weight.

#### §4. Effective Mass of the Collective Mode

The effective mass  $m^*$  of the collective mode has been estimated from the weight of the main peak of the conductivity,  $\sigma(\omega)$  in §3. In this section, we examine the effective mass of the collective mode with lowest excitation energy using a different method and compare with the result of the previous section. For this purpose, we utilize the phase Hamiltonian, which has been studied for both CDWs<sup>25)</sup> and SDWs.<sup>9,26)</sup> Using phase variable  $\theta(x)$  which describes the charge fluctuation of SDW with long wave length, the effective Hamiltonian is written as

$$H_{\text{eff}} = \int dx \left[ \frac{1}{4a} \Pi_\rho^2(x) + b \left( \frac{\partial \theta(x)}{\partial x} \right)^2 + b q_0^2 \theta^2(x) \right], \quad (4.1)$$

where  $[\theta(x), \Pi_\rho(x')] = i\delta(x - x')$ . In stead of deriving parameters,  $a$ ,  $b$  and  $q_0$  in eq. (4.1) from path integral method,<sup>27)</sup> we determine them numerically using the charge susceptibility and the spectrum of the collective mode [eq. (2.19)], which has a gap due to commensurability.

The coefficient,  $b$ , is estimated as follows. From eq. (4.1), the Green function is calculated as

$$\int_0^\beta d\tau \langle T_\tau \theta_q(\tau) \theta_{-q}(0) \rangle e^{i\omega_n \tau} = \frac{1/2}{a\omega_n^2 + b(q^2 + q_0^2)}, \quad (4.2)$$

where  $\theta_q$  is the Fourier transform of  $\theta(x)$ . It is noted that the Fourier transform of charge fluctuation with wave number  $q$  is given by  $iq\theta_q/\pi$ . Then, from eq. (4.2), the static charge susceptibility for small  $q$ , is written as

$$\chi_c(q) \simeq \left( \frac{q}{\pi} \right)^2 \langle \theta_q \theta_{-q} \rangle = \frac{1}{2\pi^2 b} \frac{q^2}{q^2 + q_0^2}. \quad (4.3)$$

The charge susceptibility is also calculated from the response function, which is defined by<sup>24)</sup>

$$\frac{-1}{2N} \int_0^\beta d\tau \langle T_\tau \Phi(q, \tau) \Phi^\dagger(q, 0) \rangle e^{i\omega_n \tau} \Big|_{i\omega_n \rightarrow \omega + i0}, \quad (4.4)$$

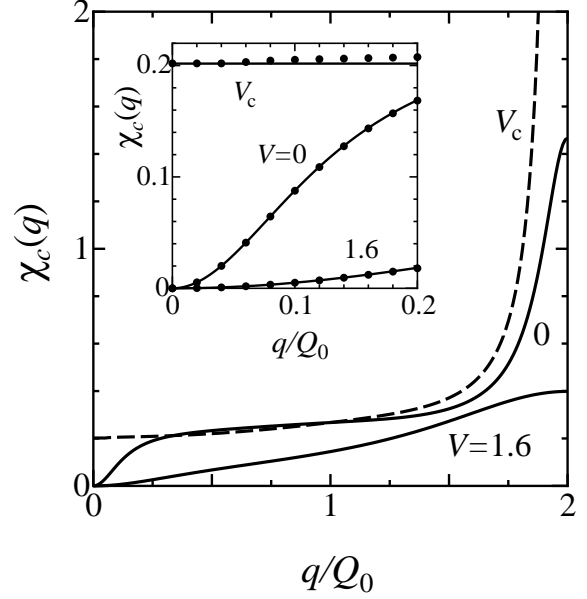


Fig. 8. The static charge susceptibility  $\chi_c$ , as a function of  $q/Q_0$ , for  $V = 0$ ,  $V_c (\simeq 0.34)$  and 1.6 where  $U = 4$ ,  $V_2 = 0$  and  $t_d = 0$ . In the inset, the numerical results of  $\chi_c(q)$  (dots) for the small  $q$  are compared with solid curves obtained from  $\chi_c(q) = q^2 [2\pi^2 b (q^2 + q_0^2)]^{-1}$ .

where  $\Phi(q)$  is given by eq. (2.20) and the response function is evaluated in the random phase approximation as  $-\overleftrightarrow{\Pi}(q, \omega) / (1 - \overleftrightarrow{U}(q) \overleftrightarrow{\Pi}(q, \omega))$ . From eq. (4.4), the static charge susceptibility is also obtained as

$$\chi_c^{\text{RPA}}(q) = \langle D_0(q) D_0(-q) \rangle, \quad (4.5)$$

where  $D_0(q) = iq\theta_q/\pi$ .<sup>26)</sup> Thus the quantity  $b$  can be obtained by comparing eq. (4.3) and eq. (4.5). In Fig. 8,  $\chi_c(q)$  as the function of  $q/Q_0$  is shown for  $V = 0$ ,  $V_c$  (dotted curve) and 1.6. One finds  $\chi_c(0) = 0$  except for  $V = V_c$  which leads to  $\chi_c(q) \neq 0$  for  $q \rightarrow 0$ . The results for  $V = V_c$  is reasonable if we note eq. (4.3) does hold and the collective mode becomes gapless, i.e.,  $q_0 = 0$ . In the inset,  $\chi_c(q)$  obtained from eq. (4.3) (solid curve) is compared with that of eq. (4.5) (dots) where  $b$  in eq. (4.3) has been determined to fit the dots. The quantity  $a$  is calculated by substituting  $b$  into the excitation spectrum obtained from eq. (2.19), which can be written as  $\omega_c(q) = \sqrt{b(q^2 + q_0^2)}/a$  for small  $q$ . In the following calculation, we use renormalized quantities defined as  $\tilde{a} \equiv 4\pi v_F a$  and  $\tilde{b} \equiv 4\pi b/v_F$  where  $v_F = \sqrt{2}$ . It is found that  $\tilde{a} = \tilde{b} = 1$  in the limit of weak interaction. We note that  $\tilde{a} = m^*/m$  since the first term of eq. (4.1) may be rewritten as  $\pi v_F (m/m^*) \Pi_\rho^2$  in a way similar to CDW.<sup>25)</sup> Thus the quantity  $\tilde{a}$  can be compared with the effective mass of the previous section, i.e., eq. (3.2).

In Fig. 9, quantities  $\tilde{a}$  and  $\tilde{b}$  as the function of  $U$  are shown by the solid curve. The open circle is obtained from eq. (3.2) where  $\eta = 0.02$  for  $U > 4$  and  $\eta = 0.02(E_2(Q_0/2) - E_1(Q_0/2))$  otherwise for numerical accuracy. The open circle coincides well with  $\tilde{a}$ . There is the visible enhancement of the effective mass  $m^*$  for  $U \gtrsim 4$ . The  $U$  dependence of  $\tilde{b}$  is also shown by the solid curve. For comparison with  $\tilde{b}$ , we show

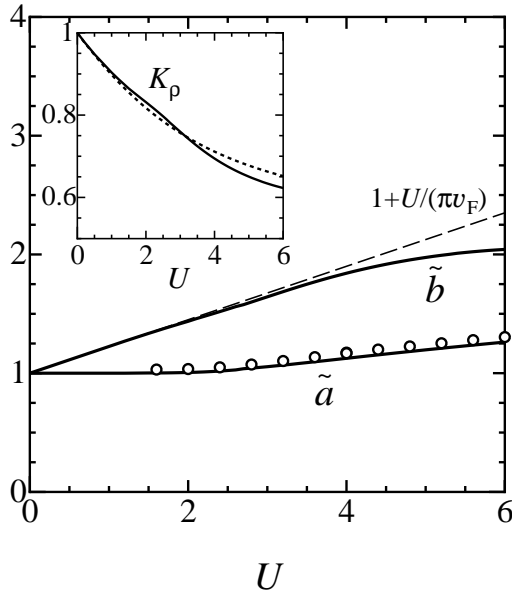


Fig. 9.  $U$  dependence of  $\tilde{a}(=4\pi v_F a)$  and  $\tilde{b}(=4\pi b/v_F)$  for  $V = V_2 = t_d = 0$  where  $a$  and  $b$  are coefficients of the effective Hamiltonian eq. (4.1). The dashed line denotes  $1+U/(\pi v_F)$ . The open circles represent  $m^*/m$  estimated from eq. (3.2). In the inset, the solid curve and the dotted curve are  $K_\rho(=1/(\tilde{a}\tilde{b})^{1/2})$  and the exact one, respectively.<sup>29)</sup>

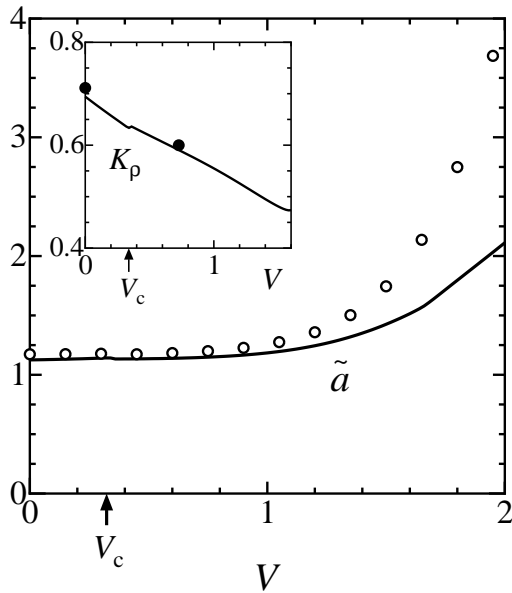


Fig. 10.  $V$  dependence of  $\tilde{a}$  (solid curve) for  $U = 4$  and  $V_2 = t_d = 0$ . The open circles represent  $m^*/m$  obtained from eq. (3.2). In the inset, solid curve and closed circle denote  $K_\rho$  and the exact result.<sup>30)</sup>

$1 + U/(\pi v_F)$  by the dashed line, which is the formula in the limit of small  $U$  and  $V = V_2 = 0$ . The solid curve deviates from the dashed line for large  $U$  due to the effect of commensurability. The good coincidence of  $\tilde{b}$  and the dashed line for small  $U$  indicates that eq. (4.1) describes well the effective Hamiltonian as seen in one-dimensional Hubbard model.<sup>28)</sup> In the inset, we show  $K_\rho(=1/(\tilde{a}\tilde{b})^{1/2})$ , a parameter for the charge fluctuation,

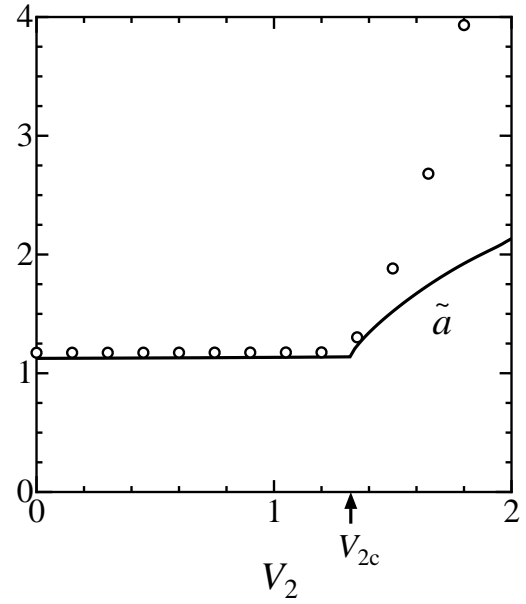


Fig. 11.  $V_2$  dependence of  $\tilde{a}$  for  $U = 4$ ,  $V = 1.2V_2$  and  $t_d = 0$ . The open circles represent  $m^*/m$  obtained from eq. (3.2).

by the solid curve where the dashed curve denotes exact one for one-dimensional Hubbard model.<sup>29)</sup> The result indicates a fact that the charge fluctuation around the mean-field ground state may be justified even quantitatively.

Further we examine  $V$  and  $V_2$  dependence of  $\tilde{a}$ . In Fig. 10, the normalized effective mass,  $m^*/m$ , as the function of  $V$  is shown by the solid curve where the circle denotes the result obtained by eq. (3.2). Both results remain almost the same and independent of  $V$  for  $V \lesssim 1$ . The mass enhancement is found for  $V (\gtrsim 1)$  which is much larger than  $V_c$ . The enhancement of  $m^*$  obtained from the response function is smaller than that obtained from the optical conductivity. In the inset,  $V$  dependence of  $K_\rho$  is shown by the solid curve where the closed circle denotes the exact result.<sup>30)</sup> It is found that the charge fluctuation obtained by the present approximation may be justified also in the presence of  $V$ .

In Fig. 11,  $V_2$  dependence of the normalized quantity  $m^*/m$  is shown where open circle denotes the result obtained by eq. (3.2). Both are almost the same and stay constant for  $V_2 < V_{2c}$ . In contrast to Fig. 10,  $m^*/m$  increases rapidly for  $V_2 > V_{2c}$ . The effective mass obtained from eq. (3.2) is larger than that of the present section. The former is the direct calculation while the latter is the result under the assumption of phase Hamiltonian of eq. (4.1). The reason for the discrepancy for large  $V$  and  $V_2$  remains unclear at present.

## §5. Dielectric Constant and Reflectivity

In order to examine the reflectivity, we calculate the dielectric constant  $\epsilon(\omega)$ , which is given by

$$\epsilon(\omega) = 1 + \frac{4\pi i}{\omega} (\sigma(\omega) + i\sigma'(\omega)) \quad , \quad (5.1)$$

where  $\sigma(\omega) + i\sigma'(\omega)$  is the dynamical conductivity defined by eq. (2.7). The imaginary part,  $\sigma'(\omega)$ , can be



calculated using the Kramers-Kronig relation with the optical conductivity  $\sigma(\omega)$ . However we calculate  $\sigma'(\omega)$  directly from eqs. (2.9) and (2.11). Actually, one obtains  $\sigma'(\omega) = \sigma'_0(\omega) + \sigma'_c(\omega)$ , where

$$\sigma'_0(\omega) = \text{Im} \left\{ \frac{2}{i\omega} [\Pi_{jj}^0(\omega) - \Pi_{jj}^0(0)] \right\}, \quad (5.2)$$

$$\sigma'_c(\omega) = \text{Im} \left\{ \frac{2}{i\omega} \Pi_{jj}^c(\omega) \right\}. \quad (5.3)$$

In Fig. 12,  $\sigma'(\omega)/e^2$  and  $\text{Re}[\epsilon(\omega)]$  are shown for  $U = 4$  and  $V = V_2 = t_d = 0$ . The quantity  $\sigma'(\omega)/e^2$  is the odd function with respect to  $\omega$ . One finds that  $\sigma'(\omega)/e^2 \propto -\omega$  for small  $\omega$  and changes the sign at  $\omega = \omega_c(0)$ . With increasing  $\omega$ ,  $\text{Re}[\epsilon(\omega)]$  increases rapidly but decreases to change the sign at the frequency,  $\omega_c(0)$ , corresponding to the main peak of  $\sigma(\omega)$ . The lower panel at  $\omega = 0$  reads  $\text{Re}[\epsilon_0(0)] = 1$  (dotted curve) and  $\text{Re}[\epsilon(0)] \simeq 62$  (solid curve). Thus, the effect of the collective mode is noticeable even at low frequency. This fact can be comprehended by the phase Hamiltonian derived in §4. From eq. (4.2), the conductivity is calculated as<sup>25)</sup>

$$\sigma(\omega) + i\sigma'(\omega) = -i\omega \frac{e^2}{\pi^2} \mathcal{D}(q=0, i\omega_n) \Big|_{i\omega_n \rightarrow \omega + i\eta}, \quad (5.4)$$

where  $\mathcal{D}(q, i\omega_n)$  is the Green function defined by the r.h.s. of eq. (4.2). Substituting eq. (5.4) into eq. (5.1), the dielectric constant is estimated as

$$\epsilon(\omega) \simeq 1 - \frac{\omega_p^2 m_c / m^*}{(\omega + i\eta)^2 - \omega_c^2(0)}, \quad (5.5)$$

where  $\omega_c(0) (= q_0 \sqrt{b/a})$  corresponds to the pole of the collective mode with lowest energy. The quantity  $\omega_p$  denotes a plasma frequency defined by

$$\int_0^\infty d\omega \sigma(\omega) = \frac{\omega_p^2}{8}. \quad (5.6)$$

It is found that eq. (5.5) explains the behavior of  $\text{Re}[\epsilon(\omega)]$ . We note that  $\epsilon(\omega) = 1 - (\omega_p^2 m_c / m) / \omega^2$  in the limit of large  $\omega$  where  $\omega_p^2 m_c / m = 8\sqrt{2} e^2$ .

In terms of the complex dielectric constant given by eq. (5.1), the reflectivity is calculated as

$$R(\omega) = \left| \frac{\sqrt{\epsilon(\omega)} - 1}{\sqrt{\epsilon(\omega)} + 1} \right|^2. \quad (5.7)$$

In Fig. 13,  $R(\omega)$  is shown for  $U = 4$ ,  $V_2 = t_d = 0$  and fixed  $V = 0, 0.4$  and  $1.6$  where the solid curve is obtained from the conductivity with the collective mode and the dotted curve is obtained from the conductivity without the collective mode. The arrow denotes the location of the plasma frequency defined by eq. (5.6) where we take  $e = 1$ . The upper panel corresponds to the result for the conventional Hubbard model with the intermediate interaction. The dotted curve exhibits the insulating behavior (i.e., small  $R(\omega)$ ) not only below the gap but also in a certain region above the gap where the cusp of the dotted curve at  $\omega \simeq 0.9$  corresponds to the gap for the single particle excitation. The solid curve shows that the collective mode enhances the reflectivity in a wide region above the gap of the collective mode

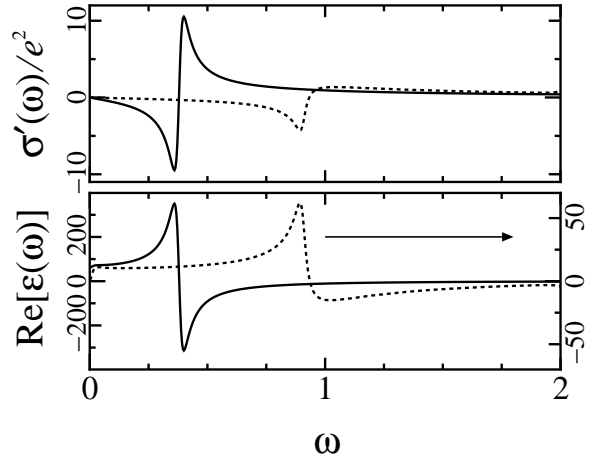


Fig. 12.  $\omega$  dependence of the imaginary part of the conductivity [ $\sigma'(\omega)$ ] and the real part of the dielectric constant [ $\epsilon(\omega)$ ] for  $U = 4$ ,  $V = V_2 = 0$  and  $t_d = 0$  where the solid curve (dotted curve) has been evaluated from  $\sigma'$  ( $\sigma'_0$ ).

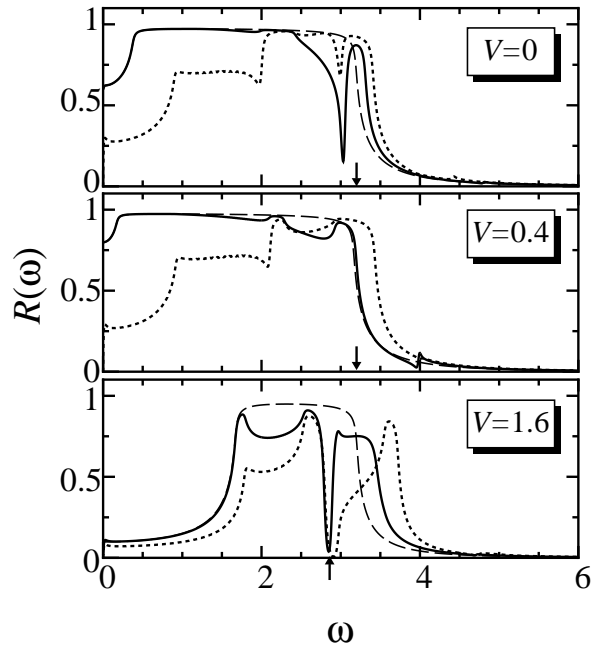


Fig. 13.  $\omega$  dependence of reflectivity  $R(\omega)$  for  $U = 4$ ,  $V_2 = 0$  and  $t_d = 0$  with the fixed  $V = 0, 0.4$  and  $1.6$  where the solid curve (dotted curve) has been evaluated from  $\sigma + i\sigma'$  ( $\sigma_0 + i\sigma'_0$ ). The arrow denotes a plasma frequency obtained from eq. (5.6). The dashed curve is calculated from eqs. (5.5) and (5.7).

[ $\omega_c(0)$ ]. This comes from the huge magnitude of the dielectric constant as seen from Fig. 12 and eq. (5.5). Here we note the following fact indicating a significant role of the collective mode with  $\omega_c(0)$ . The dashed curve in Fig. 13 is calculated from eqs. (5.5) and (5.7). One finds a good coincidence between the solid curve and the dashed curve in the wide frequency region except for high frequency regime where the effect of commensurability becomes complicated. Thus the reflectivity in the most region of frequency is determined by the collective mode with the lowest excitation energy. The sharp dip just

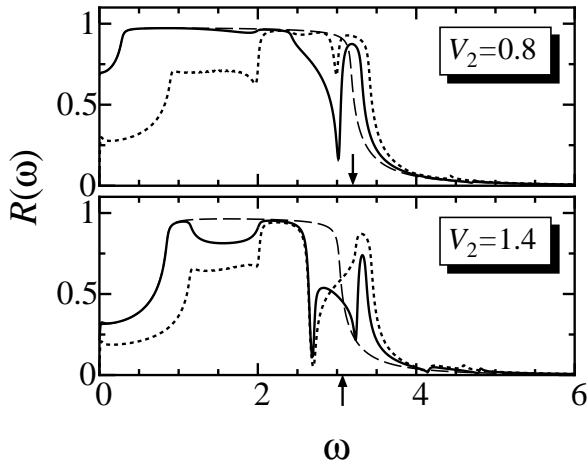


Fig. 14.  $\omega$  dependence of reflectivity  $R(\omega)$  for  $U = 4$ ,  $V = 1.2V_2$  and  $t_d = 0$  with the fixed  $V_2 = 0.8$  and  $1.4$  where the notations are the same as Fig. 13.

below the plasma frequency is found for the frequency close to the second peak of the conductivity (first panel of Fig. 4). The dip at  $\omega = 3.03$  originates in the fact that  $\text{Re}[\epsilon(\omega)]$  takes a local maximum ( $\simeq 0.13$ ) at  $\omega = 3.03$  and becomes negative for  $\omega < 3.00$  and  $3.04 < \omega$ . The effect of third peak of the conductivity is invisible in the reflectivity. The collective mode enhances the reflectivity at low frequency but suppresses it at high frequency. We note that the solid curve becomes the same as that of the free particle (i.e., the metallic state) in the limit of small  $U$ , which leads to the conductivity  $\propto 1/(i\omega - \eta)$ .

Now we examine the effect of inter-site repulsive interaction on  $R(\omega)$ . The middle panel of Fig. 13 shows the behavior for  $V$  just above  $V_c$  where the charge ordering begins to develop. Compared with the upper panel,  $R(\omega)$  is enhanced at low frequency due to the decrease of the gap of the collective mode. The small dip just below  $\omega_p$  originates in the single particle contribution while the sharp dip at  $\omega \simeq 4$  comes from the collective mode. We note the special case of  $V = V_c$  which leads to the gapless excitation of the collective mode. In this case,  $R(\omega)$  is expected to be similar to that of free particle except for the region at high frequency just below the plasma frequency as seen in the middle panel. The lower panel shows the behavior for  $V$  much larger than  $V_c$  where the charge ordering develops well. We find the insulating behavior of  $R(\omega)$  in the wide range of low frequency and still  $R(\omega) < 1$  above the gap. Thus,  $R(\omega)$  exhibits the insulating behavior for all the frequencies when the charge ordering well develops to localize the electron. Since the difference between the solid curve and the dashed curve increases with increasing  $V$ , the charge ordering reduces the effect the collective mode with  $\omega_c(0)$ . In Fig. 14,  $R(\omega)$  is shown for  $U = 4$ ,  $V/V_2 = 1.2$  and  $t_d = 0$ , and fixed  $V_2 = 0.8$  and  $1.4$  where the notations are the same as Fig. 13. The upper panel is similar to that of  $V = 0$  of Fig. 13 since both ground states are in the region (I). The lower panel is the result for the ground state in the region (III) where charge ordering comes from  $V_2$ . The insulating behavior is also found but is slightly compli-

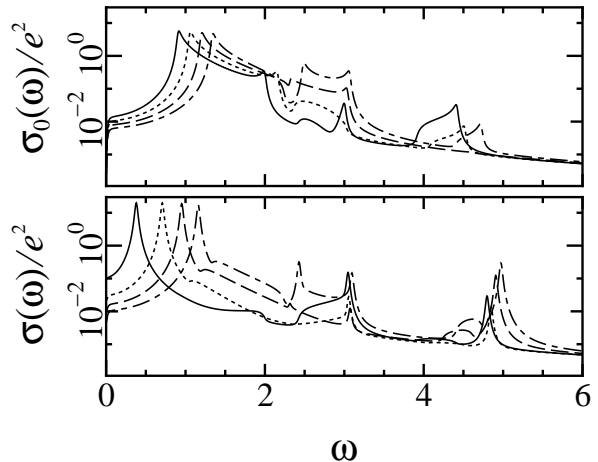


Fig. 15. Optical conductivity  $\sigma(\omega)$  is shown by the solid curve for  $t_d = 0$  (solid line),  $0.08$  (dotted line),  $0.16$  (dashed line) and  $0.24$  (dash-dotted line) with  $U = 4$ ,  $V = V_2 = 0$  and  $\eta = 0.02$  where the notations are the same as Fig. 3.

cated at high frequency. Two kinds of dip are located close to the second and third peak of the conductivity (lower panel of Fig. 6) where the origin is the same as that of Fig. 13. Based on Figs. 13 and 14, it is found that the reflectivity is suppressed sufficiently by charge ordering.

## §6. Discussion

We have examined the effect of the collective mode on the optical conductivity and the reflectivity for SDW with one-dimensional quarter-filled band using the extended Hubbard with intermediate coupling constant. The collective mode with lowest excitation energy exhibits a dominant contribution not only for the limit of small interactions but also for the intermediate coupling. When  $U$  increases to the order of band width, in addition to the main peak of the conductivity, other peaks become visible at high frequencies, which correspond to poles of the mode being active to the charge response. The effect of the collective mode decreases in the presence of the inter-site interaction, which induces charge ordering. The effective mass estimated from the weight of the main peak of the conductivity increases when the charge ordering is induced by inter-site repulsive interactions being larger than the critical value. The enhancement of effective mass is also analyzed in terms of the phase Hamiltonian. Both results agree well for weak interactions while the latter seems to underestimate in case of strong interactions. The effect of the collective mode on the reflectivity is further examined. We found that the mode with lowest excitation energy determines the reflectivity in a wide range of frequency between the single particle gap and the plasma frequency. The reflectivity in the range remains large for SDW without charge ordering while it is reduced in the presence of charge ordering.

Here we examine the effect of dimerization which is introduced in eq. (2.1a). The main effect of  $t_d$  on the ground state is to extend the region (I) into region (II)

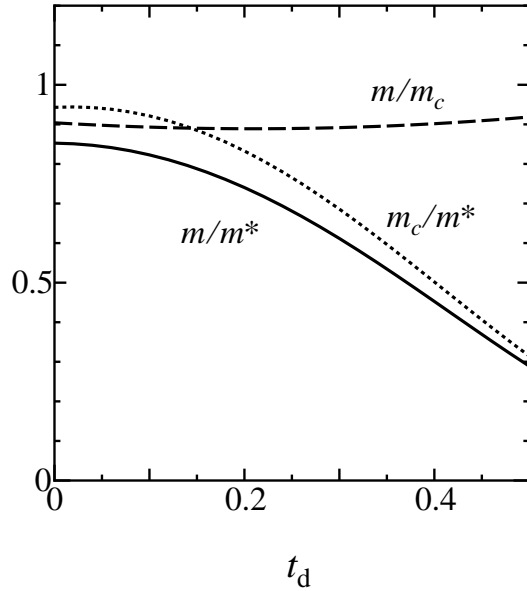


Fig. 16.  $t_d$  dependence of  $m/m^*$  (solid curve),  $m_c/m^*$  (dotted curve) and  $m/m_c$  (dashed curve) for  $U = 4$ ,  $V = V_2 = 0$  and  $\eta = 0.02$ .

(the region (III) is less effected)<sup>20)</sup> since the dimerization is compatible with the spatial variation of spin density of the region (I). The effect on the charge gap of the collective mode is rather complicated. The charge gap vanishes at the critical value,  $V_c$  corresponding to the onset of charge ordering, which increases with increasing  $t_d$ .<sup>19)</sup> Thus  $t_d$  enhances the charge gap for small  $V (< V_c)$  while  $t_d$  suppresses the charge gap for large  $V$ . In the rigorous treatment of one-dimensional Hubbard model with dimerization,<sup>13)</sup> the dimerization is crucial to obtain the main (coherent) peak. In this case, the location of the peak is shifted from zero frequency to finite frequency since the charge gap is produced only by dimerization. In the present case where SDW forms the long range order, the charge gap does exist without dimerization indicating a quantitative effect of  $t_d$  on the coherent part. However one may still expect a noticeable effect on the continuum (incoherent) part at intermediate frequency as does for the pure one-dimensional case.<sup>13)</sup> Actually we obtained the following results. Figure 15 shows the conductivity with  $t_d = 0, 0.08, 0.16$  and  $0.24$  for  $U = 4$  and  $V = V_2 = 0$  where the upper panel denotes  $\sigma_0$  and the lower one denotes  $\sigma$ . With increasing  $t_d$ ,  $\sigma_0$  moves to the regime of high frequency. For  $\sigma$ , one finds several characteristics. The weight of the first peak decreases as the function of  $t_d$  and a shoulder just above the first peak appears. The second peak decreases (increases) for  $t_d < 0.16$  ( $0.16 < t_d$ ) and the third peak decreases (increases) for  $t_d < 0.08$  ( $0.08 < t_d$ ) with increasing  $t_d$ . Another peak appears just below the second peak. These come from the interplay of the excitation of the collective mode and that of the single particle. In Fig. 16, the effective mass is shown as the function of  $t_d$ . The total weight of the conductivity ( $m_c/m$ ) remains almost constant or even slight decreasing as the function of  $t_d$  while the effective mass ( $m^*/m$ ) determined by the first pole is

increased by  $t_d$ .

Finally, we comment on the relevance of the present result to the optical experiment in the materials with the one-dimensional quarter-filled band. Although the experiment exhibits various kinds of additional effects such as the coupling to phonon and one-dimensional fluctuation in the presence of the correlation gap, it is expected that, in organic conductors, the small reflectivity of TMTTF salt compared with that of TMTSF salt could be due to the presence of charge ordering.<sup>5)</sup>

### Acknowledgments

We thank S. Sugai for useful discussion on the optical conductivity and the reflectivity.

- 
- [1] D. Jérôme and H. J. Schulz: *Adv. Phys.* **31** (1982) 299.
  - [2] G. Grüner, *Rev. Mod. Phys.* **66** (1994) 1.
  - [3] D. Quinlivan, Y. Kim, K. Holczer and G. Grüner: *Phys. Rev. Lett.* **65** (1990) 1816.
  - [4] S. Donovan, Y. Kim, L. Degiorgi, M. Dressel, G. Grüner and W. Wonneberger: *Phys. Rev. B* **49** (1994) 3363.
  - [5] V. Vescoli, L. Degiorgi, W. Henderson, Grüner, K. P. Starkey and L. K. Montgomery: *Science* **281** (1998) 1181.
  - [6] P. A. Lee, T. M. Rice, and P. W. Anderson: *Solid State Commun.* **14** (1974) 703.
  - [7] S. Takada: *J. Phys. Soc. Jpn.* **53** (1984) 2193.
  - [8] E. W. Fenton and G. C. Aers: *Low-Dimensional Conductors and Superconductors*, ed. by D. Jérôme and L. Caron (Plenum Press, New York, 1987) p. 285.
  - [9] A. Virosztek and K. Maki: *Phys. Rev. B* **37** (1988) 2028.
  - [10] P. F. Maldague: *Phys. Rev. B* **16** (1977) 2437.
  - [11] D. Baeriswyl, C. Gros and T. M. Rice: *Phys. Rev. B* **35** (1987) 8391.
  - [12] F. Mila: *Phys. Rev. B* **52** (1995) 4788.
  - [13] J. Favand and F. Mila: *Phys. Rev. B* **54** (1996) 10425.
  - [14] J. P. Pouget and S. Ravy: *J. Phys. I (France)* **6** (1996) 1501; *Synth. Met.* **85** (1997) 1523.
  - [15] S. Kagoshima, Y. Saso, M. Maesato, R. Kondo and T. Hasegawa: *Solid State Commun.* **110** (1999) 479.
  - [16] H. Seo and H. Fukuyama: *J. Phys. Soc. Jpn.* **66** (1997) 1249.
  - [17] N. Kobayashi, M. Ogata and K. Yonemitsu: *J. Phys. Soc. Jpn.* **67** (1998) 1098.
  - [18] Y. Tomio and Y. Suzumura: *J. Phys. Soc. Jpn.* **69** (2000) 796.
  - [19] Y. Suzumura: *J. Phys. Soc. Jpn.* **66** (1997) 3244.
  - [20] Y. Tomio and Y. Suzumura: *J. Phys. Soc. Jpn.* **70** (2001) 2884.
  - [21] H. Tajima: *Solid State Commun.* **113** (2000) 279.
  - [22] M. Mori and K. Yonemitsu: *Mol. Cryst. Liq. Cryst.* **343** (2000) 221.
  - [23] M. Mori and K. Yonemitsu: *J. Phys. Chem. Solids* **62** (2001) 409.
  - [24] Y. Suzumura and N. Tanemura: *J. Phys. Soc. Jpn.* **64** (1995) 2298.
  - [25] H. Fukuyama: *J. Phys. Soc. Jpn.* **41** (1976) 513.
  - [26] N. Tanemura and Y. Suzumura: *Prog. Theor. Phys.* **96** (1996) 869.
  - [27] S.A. Brazovskii and I.E. Dyaloshinskii, *Sov. Phys.-JETP* **44** (1976) 1233.
  - [28] H. Yoshioka, M. Tsuchiizu and Y. Suzumura: *J. Phys. Soc. Jpn.* **70** (2001) 762.
  - [29] H. J. Schulz: *Int. J. Mod. Phys. B* **5** (1991) 57.
  - [30] F. Mila and X. Zotos: *Europhys. Lett.* **24** (1993) 133.